processes

Article

High-Efficiency Photoresponse of Flexible Copper Oxide-Loaded Carbon Nanotube Buckypaper Under Direct and Gradient Visible Light Illumination

Lakshmanan Saravanan [1], Wei-Cheng Tu [2], Hsin-Yuan Miao [2] and Jih-Hsin Liu [2,*]

[1] Department of Physics, Saveetha School of Engineering, Saveetha Institute of Medical and Technical Sciences (SIMATS), Thandalam, Chennai 602105, Tamil Nadu, India; saravananl.sse@saveetha.com
[2] Nanoscale Electronic Materials and Energy Technologies Laboratory, Department of Electrical Engineering, Tunghai University, Taichung 40704, Taiwan; thusemidevice@gmail.com (W.-C.T.); kenymiao@thu.edu.tw (H.-Y.M.)
* Correspondence: jhliu64@thu.edu.tw

Abstract: This study used a direct dispersion and filtration technique to produce hybrid buckypaper (BP) composites of copper oxide nanoparticles (NPs) and entangled multi-walled carbon nanotubes (CNTs). The photocurrent generation of the BP sheets under two different (direct and gradient) illumination conditions was investigated by varying copper oxide loadings (10–50 wt%). The structure and morphology of the composites examined through X-ray diffraction and scanning electron microscopy (SEM) confirmed the presence of monoclinic cupric oxide nanoparticles in the CNT network. The difference in electrical resistivity between bulk-filled and surface-filled CuO-BP composites was assessed using the four-probe Hall measurement. The studies disclosed that the surface-loaded CuO on the CNT network demonstrated a superior ON and OFF response under the gradient illumination conditions with peak values of 17.69 μA and 350.04 μV for photocurrent and photovoltage, respectively. The significant photocurrent observed at zero applied voltage revealed the existence of a photovoltaic effect in the BP composites. An intense photoresponse was detected in the surface-filled sample CuO-BP composite in both illumination conditions. Additionally, at an illumination level of 150 W/m^2, wavelength-dependent photovoltaic effects on pure BP were observed using red, green, and blue filters.

Keywords: MWCNTs; buckypaper; copper oxide; photo-gradient; photocurrent

check for updates

Academic Editor: Andrea Petrella

Received: 19 December 2024
Revised: 1 January 2025
Accepted: 8 January 2025
Published: 10 January 2025

Citation: Saravanan, L.; Tu, W.-C.; Miao, H.-Y.; Liu, J.-H. High-Efficiency Photoresponse of Flexible Copper Oxide-Loaded Carbon Nanotube Buckypaper Under Direct and Gradient Visible Light Illumination. *Processes* **2025**, *13*, 188. https://doi.org/10.3390/pr13010188

Copyright: © 2025 by the authors. Licensee MDPI, Basel, Switzerland. This article is an open access article distributed under the terms and conditions of the Creative Commons Attribution (CC BY) license (https://creativecommons.org/licenses/by/4.0/).

1. Introduction

With the increasing demand for clean and renewable energy, numerous studies have explored various solar harvesting and conversion devices. Recent advancements in solar technology have focused on improving the efficiency and scalability of photovoltaic cells. In particular, various types of metal or metal oxide nanoparticles (NPs) combined with one-dimensional nanostructures for the development of unique hybrid nanomaterial systems have been investigated [1]. Owing to their exceptional mechanical strength, outstanding electrical conductivity, and exceptional flexibility, carbon-based materials—such as graphene sheets and carbon nanotube (CNT) networks—have typically been employed to create flexible electronics [2,3]. Hybridizing carbon nanotubes with metal oxide nanostructures produces a new class of multifunctional materials with substantially enhanced performances, such as photocatalysts, sensors, fuel cells, and batteries [4]. Even at high NP loadings, CNTs retain their shape and structure due to their high mechanical stability, such as substantial hardness and toughness. Recently, various hybrid composites based on CNTs with inorganic and organic materials have been reported in the literature [5–8]. CNTs combined with metal oxide NPs can be used as catalysts, sensors, data storage and processing devices, and reinforced nano-fiber materials [9,10]. Integrating metal oxides into CNTs could create conductive channels for electrons, facilitating uninterrupted electron flow, lowering electrical resistance, and thereby improving carrier mobility and electrical conductivity [11–13]. It was found that the homogeneous dispersion of metal oxide NPs in CNT substantially increased the active surface area of a CNT–metal oxide composite. At room temperature, these nanotubes are capable of the rapid transport of charge carriers across relatively long distances [14,15].

In this context, cupric oxide (CuO) nanoparticles were chosen due to their significance in photovoltaic nanodevices and solar energy applications, along with their affordability and widespread availability. CuO, among transition-metal oxides, is particularly noteworthy due to its high theoretical capacity, excellent safety profile, affordability, and non-toxicity. Numerous semiconductors, including CuO, exhibit a high absorption coefficient of sunlight while maintaining moderate extraction costs [16]. CuO, a p-type semiconductor with a narrow band gap (1.2–1.9 eV), has been frequently used among other transition metal oxides, and it has promising applications in various fields, including photodetectors, energetic materials, field emissions, supercapacitors, and photocatalysis [17,18]. CuO has an open three-dimensional shell with a direct band gap of the charge-transfer type, which can absorb light up to the near-infrared region and has high solar absorbance, low thermal emittance, and non-toxicity [19,20]. CuO NPs have excellent stability and a high carrier concentration, showing their potential for use in light-harvesting applications. However, such materials tend to have low diffusion lengths for photo-generated charge carriers; hence, the thicknesses of local absorber layers must be substantially reduced using optimized defect passivation techniques to minimize recombination losses and maximize the long-term stability of these systems [21]. Recent studies have reported the use of CNT/CuO composites for different optoelectronic applications [22–24]. There is limited information in the literature on filling CNT networks with metal oxides and metal NPs, and there is no report on the effect of filling metal oxides on the photoelectric properties of multiwalled carbon nanotube (MWCNT) buckypaper (BP). We recently focused our work on enhancing the photoelectric properties of pure CNT BP via the process of modifying the flexible sample with a plasma gradient and gradient light illumination conditions [25].

The primary aim of this work was to produce a hybrid CuO-BP composite by filling cupric oxide NPs into a macroscopic MWCNT entangled network structure. In contrast to the standard detection techniques of visible light illumination, we established a unique photoresponse behavior under two different (direct and gradient) illumination conditions. Both the photocurrent and photovoltage of CuO-filled BP composite sheets were measured in a zero-bias state. Our results demonstrate the effectiveness of integrating MWCNTs with CuO nanoparticles, highlighting the combined properties of nanoparticles and CNTs that are advantageous for fabricating flexible hybrid materials for energy harvesting applications. Furthermore, we studied the wavelength-dependent photovoltaic effect of pure BP using red, green, and blue (RGB) filters under two illumination conditions.

2. Experimental Section

2.1. Fabrication of MWCNT BP

Figure 1a,c represent the preparation conditions of CuO-loaded buckypaper (CuO-BP), an image of the buckypaper, and illumination conditions of CuO-BP samples, respectively. MWCNTs, with diameters ranging from 10 to 50 nm and lengths from 1 to 25 nm, were purchased from Scientech Corp., Taipei, Taiwan. Our previous report [26] described the process of fabricating a random network of MWCNTs (RBP) using direct suspension and filtration. In a standard experiment, MWCNTs were dispersed in deionized water, and Triton-X-100 (Burlington, MA, USA), a non-ionic surfactant that has no charge attraction to the tubes, was used to stabilize the suspension [27]. To facilitate the formation of dispersions, a high-energy (20 KHz, 63 W) sonication horn was used, and the solution was filtered in a vacuum through a nylon membrane. Following the filtering and drying process, the paper was gently peeled off and placed in an isopropyl alcohol bath to obtain a flexible, free-standing BP that was free of surfactants and had a thickness of about 70 μm, as seen in Figure 1b.

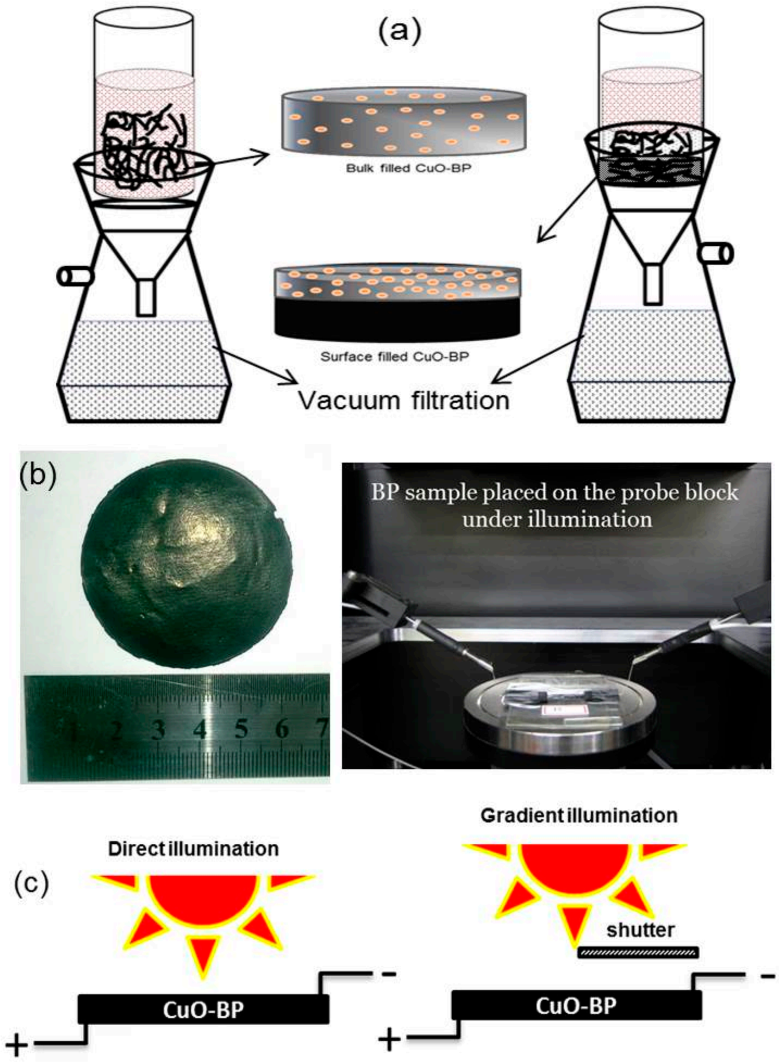

Figure 1. (**a**) Schematic of synthesizing CuO-filled MWCNT-BP composite structures (bulk-filled CuO BP and surface-filled CuO BP); (**b**) the product of flexible free-standing BP and the sample illuminating setup on the probe block of the solar simulator; and (**c**) graphical illustration of a CuO-BP sample under direct and gradient illumination conditions.

2.2. Preparation of CuO NPs and CuO-Filled BP Composites

Copper granules (3 × 3 mm) were purchased from ADMAT Midas Inc., Taipei, Taiwan, and were used to prepare cupric oxide NPs. The thermal sputtering technique was used for the preparation of CuO NPs. The samples were collected at 300 m torr in a mixed atmosphere of argon (45 sccm) and oxygen (13.5 sccm) in a 3:1 ratio within the deposition chamber, with a relative pressure of 5×10^{-5} torr. Using the same method used for BP preparation, two types of hybrid CuO-filled BP sheets were produced. Figure 1a illustrates the scheme of synthesizing CuO-BP composite structures for both the bulk-filled and surface-filled CuO BP samples. The aqueous CuO suspension was made using deionized water and added during filtration. Triton-X-100-modified nanotubes served as an effective platform for anchoring metal NPs. Thus, the CuO NPs were found to reside both in and outside of the nanotubes. CuO-BP composites were prepared using the process that was discussed in our previous report [28]. First, the CuO suspension was dispersed together entirely with an aqueous MWCNT suspension and filtered through the membrane, as illustrated on the left side of Figure 1a, and referred to as bulk-filled CuO-BP. Second, the CuO NPs were loaded on the top layer of the BP by adding the suspension of CuO NPs to the final volume of the MWCNT suspension after most of the CNT suspension was filtered out during the filtration process with the schematic shown on the right-hand side of Figure 1a, referred to as surface-filled CuO-BP. The top layer of the BP contained large quantities of CuO NPs compared with the bottom layer. The procedure was repeated for different CuO contents (10–50 wt%).

2.3. Characterization Techniques

Diffraction patterns were recorded using an X-ray diffractometer (XRD) (PHILIPS X'PERT, Tokyo, Japan) with high-intensity Cu K_α radiation (λ = 1.5406 nm). The surface morphology of hybrid CuO-BP composites was examined using JEOL JSM-7000FA field-emission scanning electron microscopy (FESEM). Energy dispersive X-ray (EDX) spectroscopic analysis of the CuO-BP composite was performed to identify the elements present in the sample. Photocurrent and photovoltage measurements were conducted on a 70-micron-thick CuO-BP composite (measuring 0.4 cm $\times$ 1.6 cm), illuminated under visible light (VL) with a power density of 1000 W/m^2 using a solar simulator from Hong-Ming Tech., Co. Ltd., New Taipei City, Taiwan. The ON/OFF photoresponse was recorded using Keithley 2410 (Keithley Instruments, Cleveland, OH, USA) as a source meter in both direct and gradient (half-light) illumination conditions. The BP sample illuminating the setup on the probe block and the scheme representing the illumination conditions (direct and gradient) are shown in Figure 1b,c, respectively. We further analyzed the current–voltage (I–V) characteristic of pure BP using red, green, and blue (RGB) filters at 650, 570, and 450 nm, respectively, with an illuminating power of 150 W/m^2 with a small bias voltage.

3. Results and Discussion

3.1. XRD Analyses

Figure 2 shows the XRD patterns of the as-prepared BP, CuO, and surface-filled CuO-BP composite sheets. Diffraction peaks were evident at 2θ = 35.43° and 38.53° with *hkl* reflections (−111) and (111), respectively, which are a match for pure cupric oxide (CuO) NPs, indicating that the particles were crystallized well in a monoclinic structure (JCPDS No. 05-0661) [29]. The average crystallite size of the CuO inside the MWCNT network was calculated to be 6.5 nm using Scherrer's formula. We found that the XRD pattern of the as-prepared pure CuO showed an additional low-intensity peak at 36.4° attributed to the Cu_2O phase. In the case of CuO-BP, in addition to the bare CuO, clear peaks with 2θ values of 25.83°, 40.48°, and 44.53° were consistent with the diffraction from the (002), (100), and (101) planes, respectively, corresponding to MWCNT and suggesting that the CuO NPs were carefully introduced on the top surface of the BP networks. Here, we observed that the surface filling of CuO NPs did not weaken the MWCNT peaks but enhanced the conductivity and subsequently increased the photo-induced carrier transfer rate in the CuO-BP composite. For pure BP, a small diffraction peak that appeared at 38° might be from the metal catalyst used during CNT synthesis.

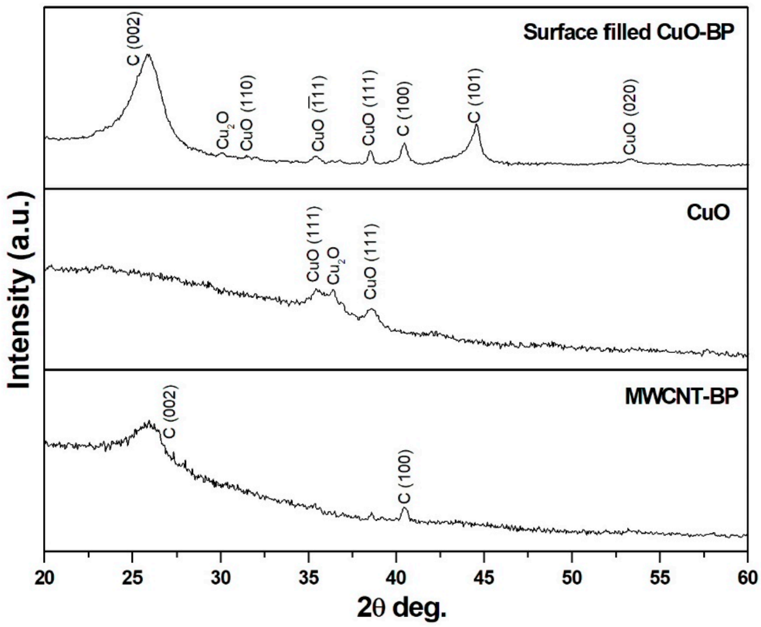

Figure 2. XRD patterns of pure BP, CuO NPs, and the CuO-BP composite.

3.2. FE-SEM Analysis

Field emission scanning electron microscopy (FE-SEM) was conducted to analyze the surface morphology of all the synthesized products. The FE-SEM micrographs of all the CuO-BP composites with different loadings of CuO NPs (10, 20, 30, and 50 wt%) are shown in Figure 3a–d, respectively. The images show the appearance of CuO particles on top of the BP networks, which indicates the effective loading of CuO NPs on the surface-filled CuO-BP composites. Increasing the CuO content (50 wt% in Figure 3d) caused a large quantity of NPs to agglomerate with CNTs in the BP composite and appear on the surface, as shown in Figure 3d. The CuO-filled BP composite contained dispersed NPs, and its reduced porosity was evident compared with the unfilled BP (pure BP) network [28], as shown by the inset in Figure 3d. High-magnified images are shown as part of the inset in Figure 3a–c to depict the presence of NPs. The EDX spectrum for the 50 wt% CuO-BP composite is depicted in Figure 3e. Only the peaks corresponding to C, Cu, and O were observed in the spectrum, revealing the presence of high CuO content in the MWCNT conducting network. Cross-sectional images are shown in Figure 3f,g to exemplify the homogeneity of nanoparticles in the CNT network.

3.3. Electrical Resistivity Measurements

Figure 4 plots the electrical resistivity of the surface-filled and bulk-filled hybrid CuO-BP composites for varying CuO concentrations in BP. The samples exhibit low resistivity values, indicating the semiconducting nature of the samples, which is ideal for generating efficient photocurrent. The graph clearly shows that the surface-filled CuO-BP samples have low resistivity values compared with the bulk-filled CuO-BP samples. The surface-filled CuO-BP sample with 20 wt% CuO exhibited a low resistivity value of 3.91×10^{-4} (Ω-m) compared with the pure BP, which exhibited a value of 4.17×10^{-4} (Ω-m). The room temperature electrical resistivity increased from 3.99×10^{-4} (Ω-m) to 5.01×10^{-4} (Ω-m) with an increase in the loading of CuO NPs from 10 to 50 wt% in pure BP. These values showed that resistivity decreased when up to 20% CuO NPs were added to the MWCNT networks. The plot showed that resistivity increased when the CuO content was further increased (>30 wt%), leading to the formation of irregular grains (or aggregates) in the CNT networks that contribute to the increased trapping and scattering of free charge carriers [30,31]. The room-temperature electrical resistivity values for bulk-filled CuO-BP samples varied from 4.65×10^{-4} (Ω-m) to 6.48×10^{-4} (Ω-m) with an increase in the CuO fraction from 10 to 50 wt%. We found that the bulk inclusion of CuO NPs in the CNT network might form an inhomogeneous mixture with conducting nanotubes, possibly due to aggregation. This aggregation increases the inter-particle resistance of the composite [32] and enhances the tendency for electron–hole recombination, subsequently reducing the transportation of charge carriers to the external circuit. This could also result in a reduction in photocurrent density due to the absence of CuO NPs deep within the network, limiting their ability to efficiently absorb sufficient light.

3.4. Photoelectrical Performances of Hybrid CuO-BP Composites

To confirm the photoelectric performance, the synthesized hybrid CuO-BP composites were fabricated as photoelectrodes (Figure 1b) and projected under different illumination conditions with zero bias voltage (Figure 1c). The photoresponse tests were conducted in a dark chamber using a halogen light source, with the distance between the lamp and the CNT film set to approximately 16 cm. Light illumination was switched ON and OFF by a chopper. Figures 5 and 6 illustrate the time-dependent photoresponse behaviors of the hybrid CuO-BP samples, depicting the photocurrent and photovoltage outputs, respectively. The CuO NP-filled MWCNT network (BP) composites yielded a higher photo-conversion compared with the pure MWCNT-BP. We predict that the increase in the photo-induced emission current was associated with the semiconducting properties of the CuO NPs embedded within the MWCNT network. Therefore, the observed increase in the photocurrent could be attributed to the increase in the carrier density caused by the excitation of the incident photons. The bare CuO, with its narrow band gap, exhibited a high tendency to excite the valence electrons through illumination, as well as a tendency to recombine the generated electrons and holes. In contrast, the CuO/MWCNT composite exhibited an appropriate band energy structure [24] and a large electron storage capacity. As a result, CNTs can accept photo-excited electrons from nanostructured semiconductive oxide, which hinders the electron–hole recombination rate and enhances photoelectrical conversion efficiency. Specifically, the high conductivity along the tube axis of CNTs enabled these materials to spatially direct the flow of photo-generated electrons and facilitate both charge injection and extraction. This implies that MWCNTs serve as an excellent conducting material and accelerate the electron transfer process. The conductive structure of CNT scaffolds is believed to promote the separation of photo-generated electron–hole pairs through the formation of heterojunctions at the CNT semiconductor interface. A recent study [24] reported that when the contacts composed of different materials with different dimensions are excited by light or heat, both the heterojunctions and heterodimensional effects must be taken into consideration simultaneously. Thus, the strong binding interaction between oxide NPs and CNTs in a surface-filled CuO-BP photoelectrode can efficiently accelerate electron transfer and enhance photoelectric performance.

Figure 5a,b correspond to the photocurrent profiles of surface-filled CuO-BP under two illumination (direct and gradient) conditions with multiple ON/OFF cycles. Under the gradient illumination, the photocurrent of the composite shown in Figure 5b increased to 17.69 μA for 20 wt% CuO-BP compared with the sample under direct illumination with a value of 6 μA for 30 wt% CuO-BP, as shown in Figure 5a. The rise and decay times observed for the 20 wt% CuO-BP composites were approximately 63 s and 68 s, respectively, and were repeatable several times without any appreciable change. The experimental results indicated that under gradient illumination, the low content of CuO incorporated into the BP network provided a considerable number of mobile charge carriers, which significantly increased the light absorption behavior to generate an efficient photocurrent. The MWCNT network loaded with 20 wt% CuO NPs demonstrated improved electrical conductivity and accelerated electron transfer, as indicated by the induced photoresponse and confirmed through electrical resistivity measurements. It has been reported that the charge transfer resistance under illumination is lower than that in the dark for photoelectrode materials. This could be due to the increased electronic conductivity of photoelectrodes under illumination [33].

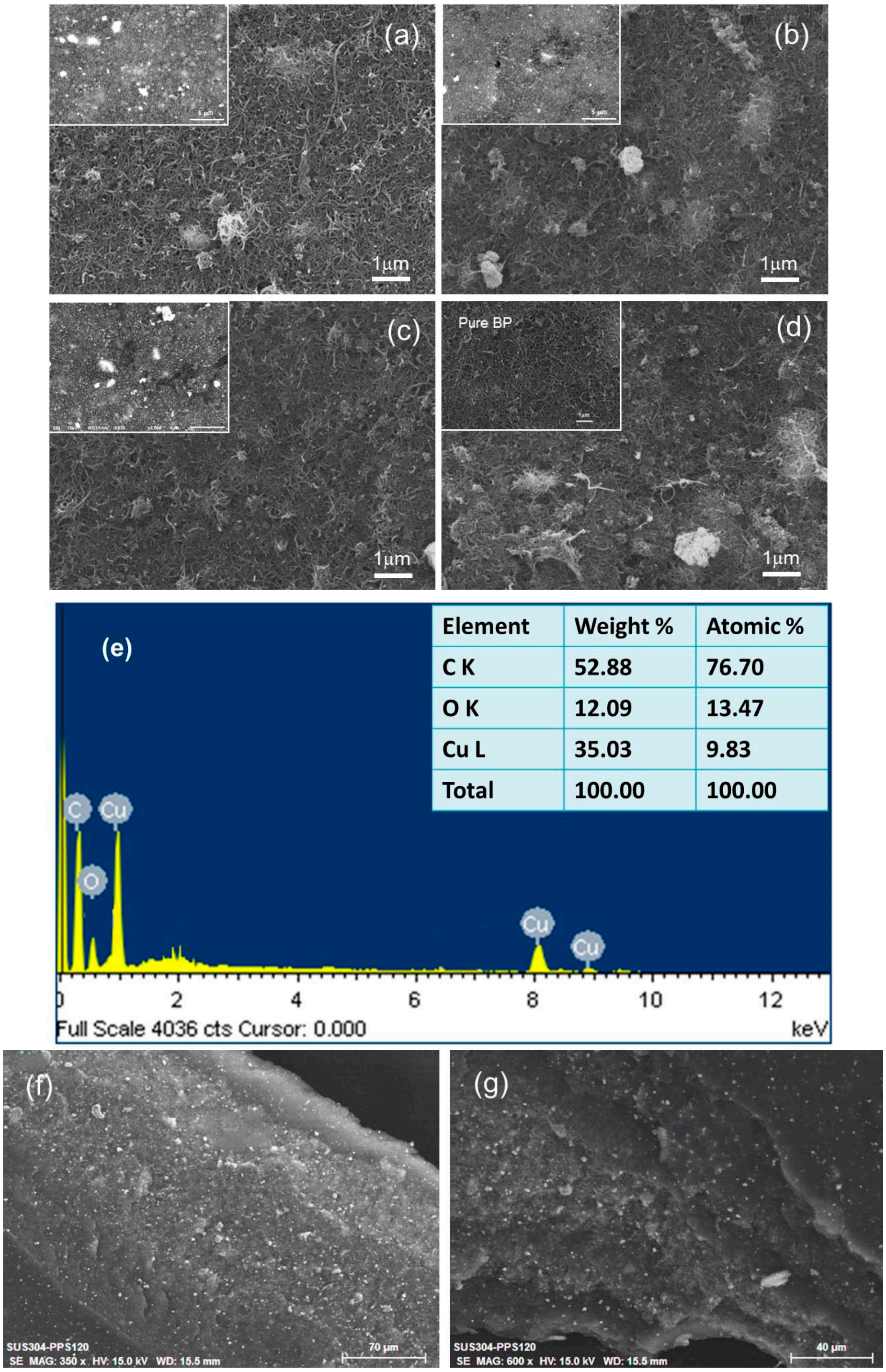

Element	Weight %	Atomic %
C K	52.88	76.70
O K	12.09	13.47
Cu L	35.03	9.83
Total	100.00	100.00

Figure 3. FESEM images of (**a**) 10, (**b**) 20, (**c**) 30, and (**d**) 50 wt% surface-filled CuO-BP composites (inset shown for pure BP) and (**e**) EDX spectrum for the 50 wt% CuO-BP sample. The inset in (**a**,**b**,**c**) represents the CuO nanoparticles in the CNT network. (**f**,**g**) Cross-section images of 30 wt% and 50 wt% CuO NPs loaded with BP.

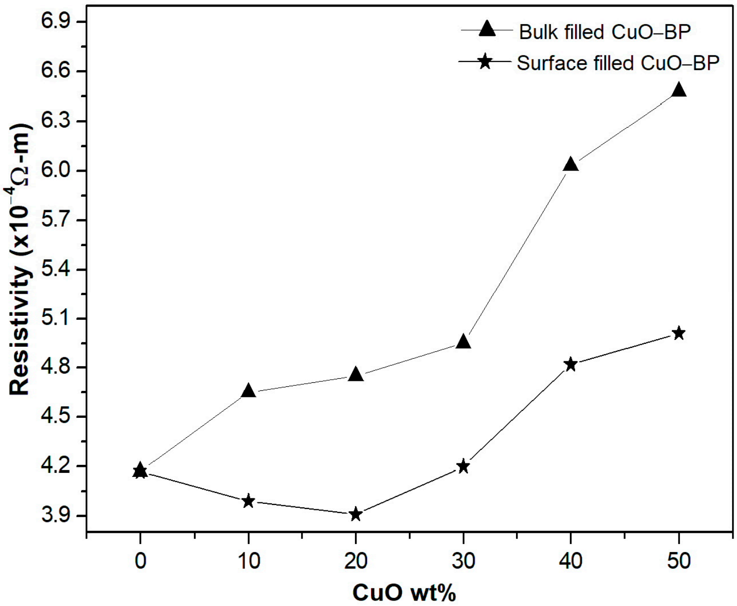

Figure 4. Variation in the electrical resistivity of both bulk-filled and surface-filled CuO-BP composites with different CuO contents.

Figure 6a,b display the photovoltage profiles of surface-filled CuO-BP under direct and gradient conditions, respectively. Figure 6b shows a higher photovoltage value of 350.04 μV for 20 wt% CuO-BP in gradient illumination, compared with the value of 120 μV for the 30 wt% CuO-BP sample under direct illumination. The nearly triple output values indicated the improved charge collection efficiency of the MWCNT network in the surface-filled hybrid composites. In our previous report [28], we proposed that gradient illumination produces a junction layer in the BP composite sheet to control the number of charge carriers and their flow in between the junction to enhance the production efficiency of the photocurrent. For the sample under direct illumination shown in Figure 1c, numerous carriers generated by the CuO produced a scattering effect among them and constrained the flow of the charge carriers inside the network, causing high electronic resistance inside the CuO-BP composites [34] and resulting in unstable photoresponse behavior, as shown in Figures 5a and 6a. The results showed that the interfacial combination of this semiconductor oxide and MWCNTs is essential for efficient charge transfer and the high activity of the hybrid composites. It has been previously observed that the electric field in a random network of MWCNTs can arise from various local Schottky junctions, such as those forming at the interfaces between semiconducting and metallic nanotubes or within the same tube [35]. Regarding the hybrid CuO-BP composite, we infer that the existence of CuO NPs forms a local interface in the nanotube network to produce Schottky junctions and, thus, improve the charge transfer. Conversely, for bulk filling, we suggest that the excess NPs inside the networks deteriorate the performance of the photoresponse by destroying the network structure of the CNT matrix and reducing the conductivity of the electrode.

Figure 7a,b, respectively, show the variation in photocurrent generation for bulk-filled and surface-filled CuO-BP composites under two illumination conditions. The figures show that the surface-loaded CuO-MWCNT network significantly enhanced photovoltaic performance. This improvement was attributed to the increased surface area and the greater number of photo-induced carrier sites on the photoelectrode surface in comparison to the bulk-filled CuO-BP composites. We determine that the CuO NPs inside the networks of the bulk-filled samples are unable to absorb all the photon energy illuminating the sample, which causes a decrease in the number of photo-induced carriers compared to the surface-filled samples. There might also be the possibility of faster recombination in CuO NPs in bulk-filled samples before the carriers are transported through the nanotubes to generate a photocurrent. A bar chart comparison of the photocurrent output for CuO NP-filled BP under gradient illumination is shown in Figure 7c. A comparison of the photocurrent output for various copper oxide–CNT and copper oxide–graphene composites from the literature is provided in Table 1 [24,36–39].

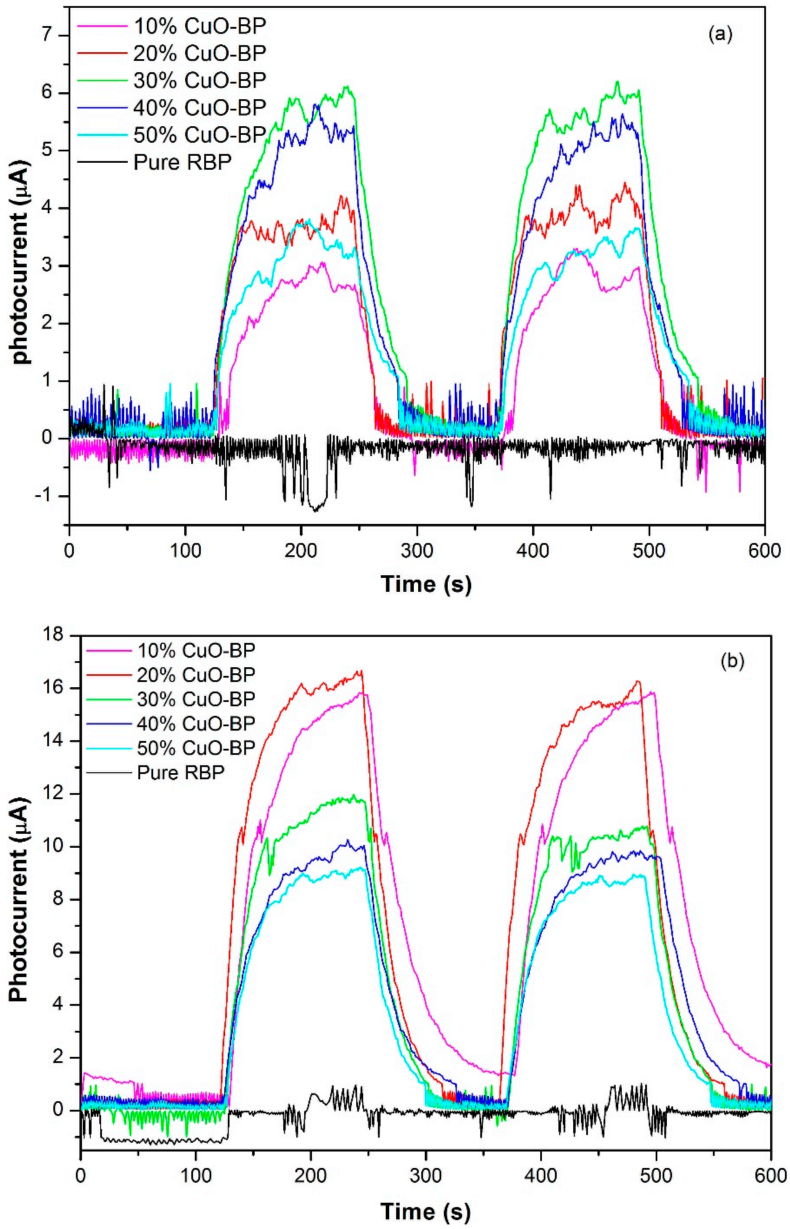

Figure 5. Time-resolved ON/OFF photocurrent generation of surface-filled CuO-BP composites with zero bias under (**a**) direct and (**b**) gradient illumination conditions.

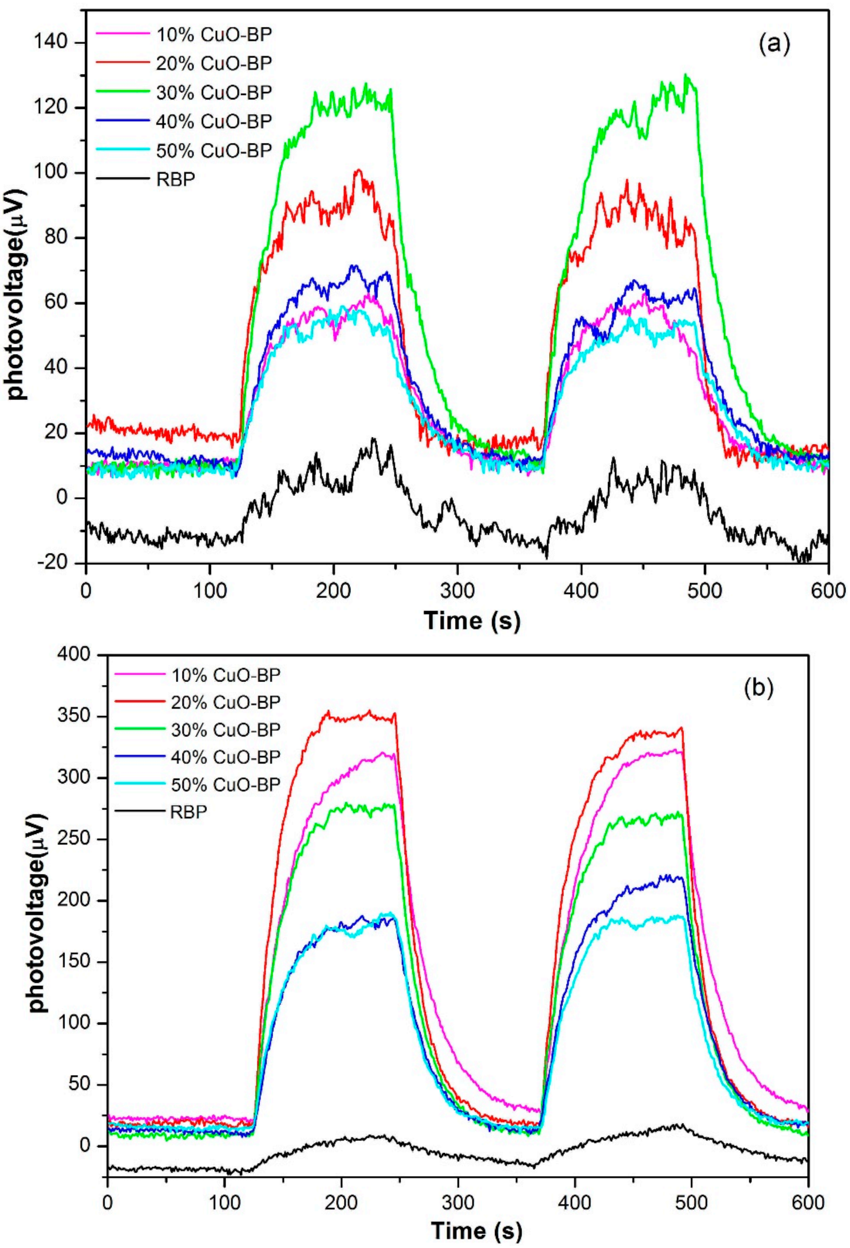

Figure 6. Time-resolved ON/OFF photovoltage output of surface-filled CuO-BP composites under (**a**) direct and (**b**) gradient illumination conditions.

Table 1. Comparison table for the photocurrent output for the copper oxide–CNT and copper oxide–graphene composites.

Sample	Photocurrent Value	Bias Voltage	Ref.
Pure CuO	2.38 μA	30 V	36
DWCNT-CuO	32 nA	1 V	24
Cu-MWCNT	900 nA	12 mV	37
Cu_2O-graphene	1.9 mA	0.05 V	38
CNT/Cu_2O film on ITO	450 μA	0.1 V	39
CuO-BP	17.69 μA	0 V	This work

Figure 8a–c show the I–V characteristics of the pure BP that were subjected to direct and gradient illumination at 650, 570, and 450 nm using RGB filters, respectively, with the bias voltage ranging from −2 to 2 V. In all cases, linear relationships were observed between the current and the voltage. The strong bias dependence in the photoconduction in Figure 8

could be due to the fact that bias voltage facilitates the separation of bound electron–hole pairs. Under both illumination conditions, the sample showed sharp increases in current as the voltage increased. This indicates that the optically generated carriers were swept down because of their tilted potential, and the degree of the tilt was clearly a function of the applied voltage. The trend of the increase in current appears highly similar to all filters. When the illumination condition was altered from direct to gradient, as shown in Figure 8, the measured photocurrent at a given bias voltage shifted upward consistently (inset) at the frequency of the light chopper. A close-up of the two I–V curves is shown in the inset of Figure 8 for different wavelengths.

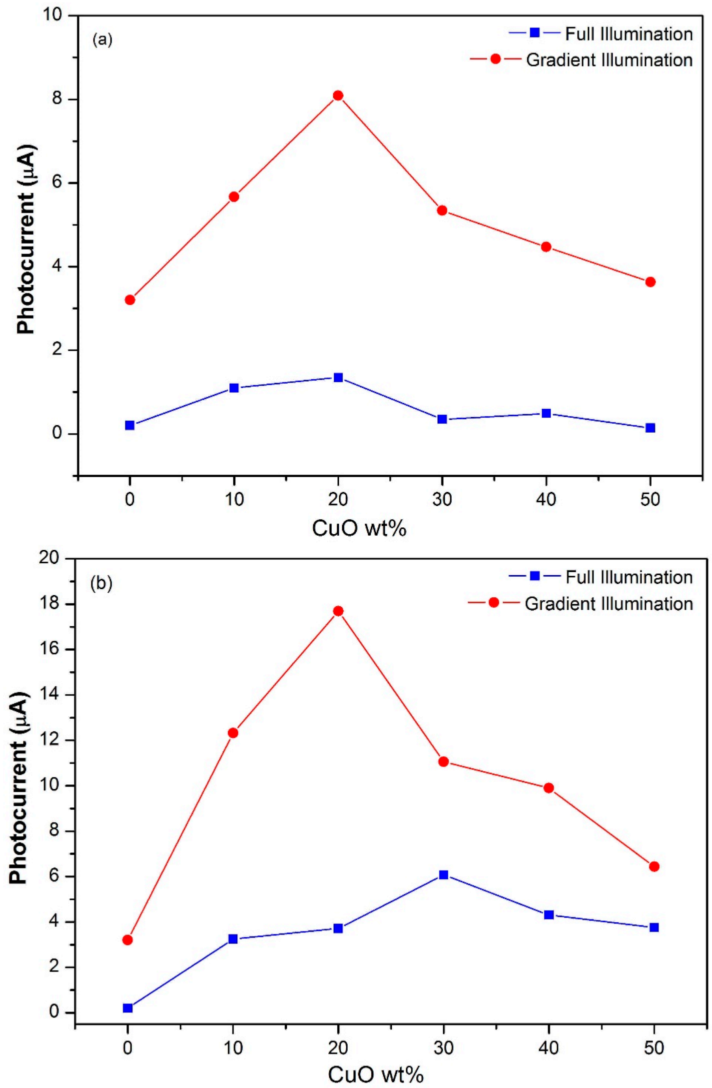

Figure 7. *Cont.*

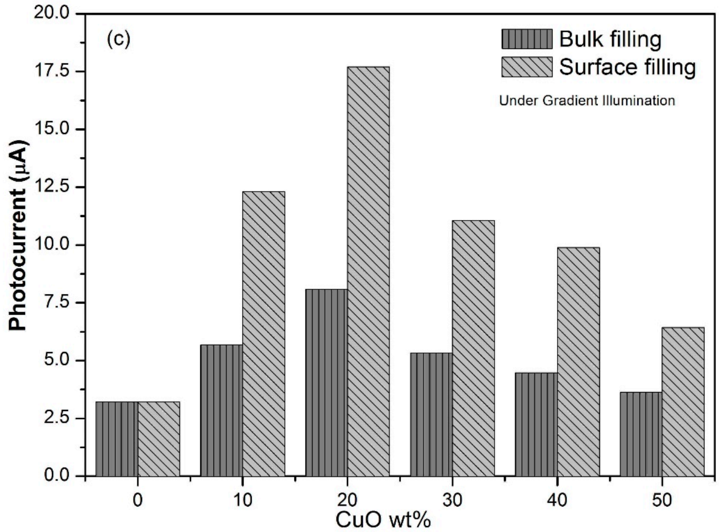

Figure 7. Variation in the photoresponse behavior for (**a**) bulk-filled and (**b**) surface-filled CuO-BP composites under both illumination conditions and (**c**) a bar chart comparison of CuO NP-filled BP under gradient illumination.

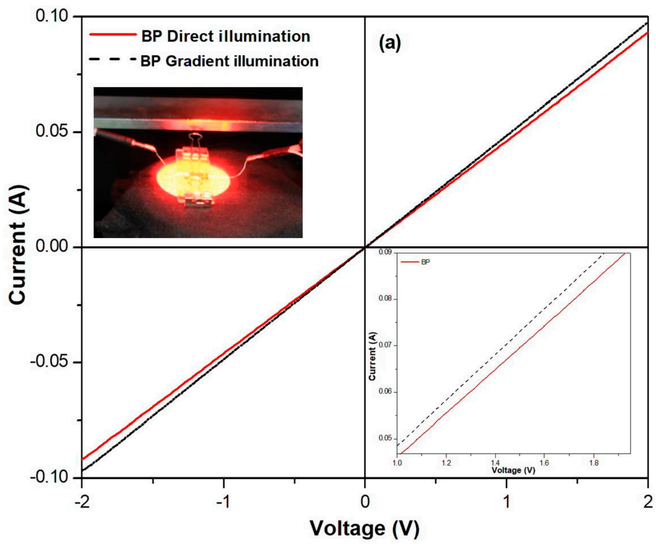

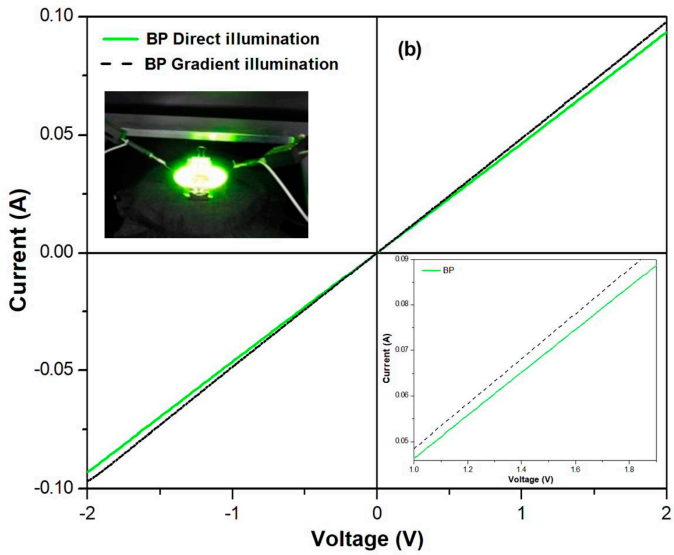

Figure 8. *Cont.*

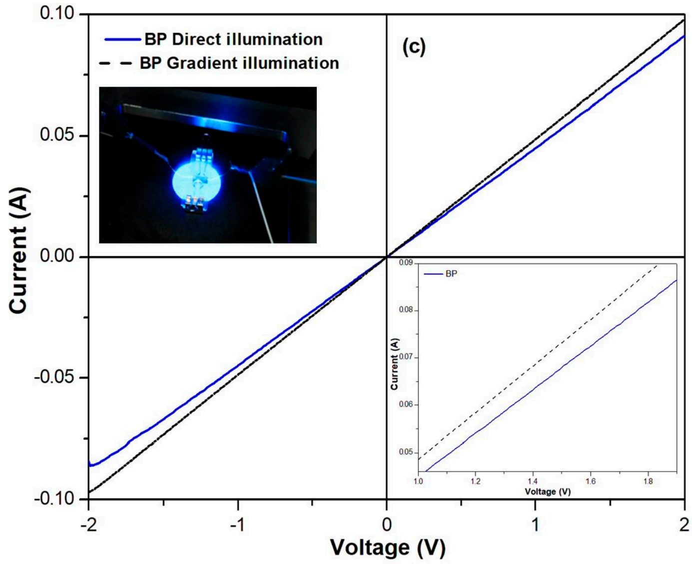

Figure 8. I–V characteristics under illumination at (**a**) 650, (**b**) 570, and (**c**) 450 nm, respectively, using RGB filters with a bias voltage range of −2 to 2 V. The inset shows (top left) the BP sample under illumination with RGB filters and (bottom right) close-up curves under two illumination conditions.

4. Conclusions

This study highlights the possible fabrication of hybrid CuO-BP composites containing monoclinic cupric oxide NPs dispersed in the multiwalled carbon nanotube entangled network (BP). This work demonstrates the effect of two types of visible light illumination—direct and gradient—on photo-induced current generation from a CuO-BP composite sheet. The MWCNT network filled with CuO NPs could easily transport the photo-generated electrons from CuO particles and inhibit the recombination of the electron–hole pairs. From XRD, we inferred that the uniform dispersion of CuO NPs in the MWCNT network is in the nanoscale regime with an average particle size of 6.5 nm. FESEM images show evidence of the presence of CuO particles in the CNT entangled network, and a large amount of CuO particles are clearly visible when increasing the content to 50%. The surface-filled CuO-BP flexible sheet exhibited a higher photoresponse with 17.69 μA and 350.04 μV for the photocurrent and photovoltage, respectively, under gradient illumination conditions. The surface-filled CuO-BP composite exhibited a higher photovoltage value of 350.04 μV for 20 wt% CuO NPs loaded in BP. Current findings demonstrate that the outstanding performance of this unique hybrid composite material is largely dependent on the interfacial interaction between the metal oxides and CNTs. We conclude that our macroscopic two-dimensional (2D) CuO-loaded MWCNT flexible network in the hybrid composite form offers high conductivity as a photoelectrode and facilitates rapid charge carrier exchange between CuO and the current collector (CNTs). These results demonstrate that optimized copper oxide nanoparticles in buckypaper deliver excellent photoresponsivity under visible light illumination.

Author Contributions: Investigation, L.S.; Methodology, W.-C.T.; Supervision, H.-Y.M. and J.-H.L. All authors have read and agreed to the published version of the manuscript.

Funding: This research was funded by Tunghai University and the National Science and Technology Council, Taiwan, grant number NSTC 112-2622-E-029-007.

Data Availability Statement: The original contributions presented in this study are included in the article. Further inquiries can be directed to the corresponding author.

Conflicts of Interest: The authors declare that they have no conflicts of interest.

References

1. Walter, E.C.; Murray, B.J.; Favier, F.; Penner, R.M. "Beaded" Bimetallic nanowires: Wiring nanoparticles of metal 1 using nanowires of metal 2. *Adv. Mater.* **2003**, *15*, 396–399. [CrossRef]
2. Dillon, A.C. Carbon Nanotubes for Photoconversion and Electrical Energy Storage. *Chem. Rev.* **2010**, *110*, 6856–6872. [CrossRef]
3. Dikin, D.A.; Stankovich, S.; Zimney, E.J.; Piner, R.D.; Dommett, G.H.B.; Evmenenko, G.; Nguyen, S.T.; Ruoff, R.S. Preparation and characterization of graphene oxide paper. *Nature* **2007**, *448*, 457–460. [CrossRef] [PubMed]
4. Chung, Y.-C.; Julistian, A.; Saravanan, L.; Chen, P.-R.; Xu, B.-C.; Xie, P.-J.; Lo, A.-Y. Hydrothermal Synthesis of CuO/RuO_2/MWCNT Nanocomposites with Morphological Variants for High Efficient Supercapacitors. *Catalysts* **2022**, *12*, 23. [CrossRef]
5. Feng, J.; Xiong, S.; Wang, Y. Atomic layer deposition of hybrid metal oxides on carbon nanotube membranes for photodegradation of dyes. *Compos. Commun.* **2019**, *12*, 39–46. [CrossRef]
6. Picuntureo, M.; García-Merino, J.A.; Villarroel, R.; Hevia, S.A. The Synthesis of Sponge-like V_2O_5/CNT Hybrid Nanostructures Using Vertically Aligned CNTs as Templates. *Nanomaterials* **2024**, *14*, 211. [CrossRef] [PubMed]
7. Wan, L.; Deng, C.; Zhao, Z.-Y.; Zhao, H.-B.; Wang, Y.-Z. A titanium dioxide–carbon nanotube hybrid to simultaneously achieve the mechanical enhancement of natural rubber and its stability under extreme frictional conditions. *Mater. Adv.* **2021**, *2*, 2408–2418. [CrossRef]
8. Pathak, P.; Park, S.; Cho, H.J. A Carbon Nanotube–Metal Oxide Hybrid Material for Visible-Blind Flexible UV-Sensor. *Micromachines* **2020**, *11*, 368. [CrossRef] [PubMed]
9. Sharafeldin, I.; Rios, S.G.; Ahmed, N.; Alvarado, M.; Vilanova, X.; Allam, N.K. Metal-decorated carbon nanotubes-based sensor array for simultaneous detection of toxic gases. *J. Environ. Chem. Eng.* **2021**, *9*, 104534. [CrossRef]
10. Liu, S.; Shen, Q.; Cao, Y.; Gan, L.; Wang, Z.X.; Steigerwald, M.L.; Guo, X. Chemical functionalization of single-walled carbon nanotube field-effect transistors as switches and sensors. *Coord. Chem. Rev.* **2010**, *254*, 1101–1116. [CrossRef]
11. Zhang, W.D.; Xu, B.; Jiang, L.C. Functional hybrid materials based on carbon nanotubes and metal oxides. *J. Mater. Chem.* **2010**, *20*, 6383–6391. [CrossRef]
12. Huang, Q.; Gao, L. Multiwalled carbon nanotube/$BaTiO_3$ nanocomposites: Electrical and rectification properties. *Appl. Phys. Lett.* **2005**, *86*, 123104. [CrossRef]
13. Flahaut, E.; Peigney, A.; Laurent, C.; Marliere, C.; Chasteland, F.; Rousset, A. Carbon nanotube–metal–oxide nanocomposites: Microstructure, electrical conductivity and mechanical properties. *Acta Mater.* **2000**, *48*, 3803–3812. [CrossRef]
14. Berger, C.; Yi, Y.; Wang, Z.L.; de Heer, W.A. Multiwalled carbon nanotubes are ballistic conductors at room temperature. *Appl. Phys. A* **2002**, *74*, 363–365. [CrossRef]
15. Javey, A.; Jing, G.; Qian, W.; Lundstrom, M.; Dai, H. Ballistic carbon nanotube field-effect transistors. *Nature* **2003**, *424*, 654–657. [CrossRef] [PubMed]
16. Wadia, C.; Alivisatos, A.P.; Kammen, D.M. Materials Availability Expands the Opportunity for Large-Scale Photovoltaics Deployment. *Environ. Sci. Technol.* **2009**, *43*, 2072–2077. [CrossRef] [PubMed]
17. Raizada, P.; Sudhaik, A.; Patial, S.; Hasija, V.; Khan, A.A.P.; Singh, P.; Gautam, S.; Kaur, M.; Nguyen, V.-H. Engineering nanostructures of CuO-based photocatalysts for water treatment: Current progress and future challenges. *Arab. J. Chem.* **2020**, *13*, 8424–8457. [CrossRef]
18. Song, H.J.; Seo, M.H.; Choi, K.W.; Jo, M.-S.; Yoo, J.-Y.; Yoon, J.-B. High-Performance Copper Oxide Visible-Light Photodetector via Grain-Structure Model. *Sci. Rep.* **2019**, *9*, 7334. [CrossRef]
19. Ito, T.; Yamaguchi, H.; Okabe, K.; Masumi, T. Single-crystal growth and characterization of Cu_2O and CuO. *J. Mater. Sci.* **1998**, *33*, 3555–3566. [CrossRef]
20. Ghisen, J. Electronic-structure of Cu_2O and CuO. *Phys. Rev. B.* **1988**, *38*, 11322–11330. [CrossRef]
21. Dittrich, T.; Belaidi, A.; Ennaoui, A. Concepts of inorganic solid-state nanostructured solar cells. *Sol. Energy Mater. Sol. Cells* **2011**, *95*, 1527–1536. [CrossRef]
22. Kumar, A.; Singh, A.; Kumar, D.; Garg, A.; Dutta, V.; Swami, S.K.; Chaturvedi, N.; Kumar, M. Spray deposited carbon nanotube embedded ZnO as an electrons transport layer in inverted organic solar cells. *Hybrid Adv.* **2023**, *4*, 100088. [CrossRef]
23. Tang, H.; Cao, Q.; He, Z.; Wang, S.; Han, J.; Li, T.; Gao, B.; Yang, J.; Deng, D.; Li, X. SnO_2–Carbon Nanotubes Hybrid Electron Transport Layer for Efficient and Hysteresis-Free Planar Perovskite Solar Cells. *Sol. RRL* **2019**, *4*, 1900415. [CrossRef]
24. Xu, J.; Sun, J.L.; Wei, J.; Xu, J. The wavelength dependent photovoltaic effects caused by two different mechanisms in carbon nanotube film/CuO nanowire array heterodimensional contacts. *Appl. Phys. Lett.* **2012**, *100*, 251113–2511135. [CrossRef]
25. Yang, C.-C.; Shen, P.-Y.; Miao, H.-Y.; Huang, C.-Y.; Lin, S.-H.; Weng, J.-H.; Saravanan, L.; Liu, J.-H. Enhancing the Photoelectric Properties of Flexible Carbon Nanotube Paper by Plasma Gradient Modification and Gradient Illumination. *Processes* **2024**, *12*, 1449. [CrossRef]
26. Liu, J.H.; Miao, H.Y.; Saravanan, L.; Wang, L.C.; Tsai, R.H. Fabrication of metal alloy-deposited flexible MWCNT buckypaper for thermoelectric applications. *J. Nanomater.* **2013**, *2013*, 635647–6356476. [CrossRef]

27. Li, N.; Zhang, S.; Ma, H.; Zheng, L. Role of solubilized water in micelles formed by triton x-100 in 1-butyl-3-methylimidazolium ionic liquids. *Langmuir* **2010**, *26*, 9315–9320. [CrossRef] [PubMed]
28. Liu, J.H.; Saravanan, L. Zinc oxide loaded MWCNT buckypaper for the efficient photocurrent generation. *Mater. Lett.* **2014**, *134*, 30–33. [CrossRef]
29. Tian, J.; Li, H.; Xing, Z.; Wang, L.; Luo, Y.; Asiri, A.M.; Youbi, A.O.A.; Sun, X. One-pot green hydrothermal synthesis of CuO–Cu_2O–Cu nanorod-decorated reduced graphene oxide composites and their application in photocurrent generation. *Catal. Sci. Technol.* **2012**, *2*, 2227–2230. [CrossRef]
30. Serin, T.; Yildiz, A.; Sahin, S.H.; Serin, N. Extraction of important electrical parameters of CuO. *Phys B: Condens. Matter* **2011**, *406*, 575–578. [CrossRef]
31. Serin, T.; Yildiz, A.; Sahin, S.H.; Serin, N. Multiphonon hopping of carriers in CuO thin films. *Phys. B: Condens. Matter* **2011**, *406*, 3551–3555. [CrossRef]
32. Lee, D.H.; Kim, D.W.; Park, J.G. Enhanced rate capabilities of nanobrookite with electronically conducting MWCNT networks. *Cryst. Growth Des.* **2008**, *8*, 4506–4510. [CrossRef]
33. Zhang, Z.; Yuan, Y.; Liang, L.; Cheng, Y.; Xu, H.; Shi, G.; Jin, L. Preparation and photoelectrochemical properties of a hybrid electrode composed of polypyrrole encapsulated in highly ordered titanium dioxide nanotube array. *Thin Solid Films* **2008**, *516*, 8663–8667. [CrossRef]
34. Zhang, Y.; Sun, X.; Pan, L.; Li, H.; Sun, Z.; Sun, C.; Tay, B.K. Carbon nanotube–ZnO nanocomposite electrodes for supercapacitors. *Solid State Ion.* **2009**, *180*, 1525–1528. [CrossRef]
35. Fuhrer, M.S.; Nygård, J.; Shih, L.; Forero, M.; Yoon, Y.G.; Mazzoni, M.S.C.; Choi, H.J.; Ihm, J.; Louie, S.G.; Zettl, A.; et al. Crossed nanotube junctions. *Science* **2000**, *288*, 494–497. [CrossRef]
36. Ko, Y.H.; Nagaraju, G.; Lee, S.H.; Yu, J.S. Facile preparation and optoelectronic properties of CuO nanowires for violet light sensing. *Mater. Lett.* **2014**, *117*, 217–220. [CrossRef]
37. Scarselli, M.; Scilletta, C.; Tombolini, F.; Castrucci, P.; Diociaiuti, M.; Casciardi, S.; Gatto, E.; Venanzi, M.; De Crescenzi, M. Multiwall Carbon Nanotubes Decorated with Copper Nanoparticles: Effect on the Photocurrent Response. *J. Phys. Chem. C* **2009**, *113*, 5860–5864. [CrossRef]
38. Kecsenovity, E.; Endrődi, B.; Tóth, P.S.; Zou, Y.; Dryfe, R.A.W.; Rajeshwar, K.; Janáky, C. Enhanced Photoelectrochemical Performance of Cuprous Oxide/Graphene Nanohybrids. *J. Am. Chem. Soc.* **2017**, *139*, 6682–6692. [CrossRef] [PubMed]
39. Kecsenovity, E.; Endrődi, B.; Pápa, Z.; Hernádi, K.; Rajeshwar, K.; Janáky, C. Decoration of Ultra-Long Carbon Nanotubes with Cu_2O Nanocrystals: A Hybrid Platform for Enhanced Photoelectrochemical CO_2 Reduction. *J. Mater. Chem. A* **2016**, *4*, 3139–3147. [CrossRef]

Disclaimer/Publisher's Note: The statements, opinions and data contained in all publications are solely those of the individual author(s) and contributor(s) and not of MDPI and/or the editor(s). MDPI and/or the editor(s) disclaim responsibility for any injury to people or property resulting from any ideas, methods, instructions or products referred to in the content.